

Assessment of 2D-Transport/1D-Diffusion Approximations in a Pin Resolved Variational Nodal Method for PWR Calculations

Tengfei Zhang,^{a*} Yongping Wang,^a E. E. Lewis,^b M. A. Smith,^c W. S. Yang^d and Hongchun Wu^a

^a Xi'an Jiaotong University, Xi'an, Shannxi, 710049, China, xfempty@gmail.com, wang3329@purdue.edu, hongchun@mail.xjtu.edu.cn

^b Northwestern University, 2145 Sheridan Road Tech, Evanston, IL, 60208-3109, U.S., e-lewis@northwestern.edu

^c Argonne National Laboratory, 700 South Cass Avenue, Lemont, IL, 60439, U.S., masmith@anl.gov

^d Purdue University, 400 Central Drive, West Lafayette, IN, 47907, U.S., yang494@purdue.edu

Abstract - An assessment of the approximation in a two-dimensional transport/one-dimensional diffusion (2D/1D) variational nodal method for pin-resolved pressurized water reactor (PWR) core calculations is presented. The derivation of the response matrices on which the solution algorithms are based is modified to include a more efficient inclusion of the quasi-reflected interface conditions that are essential to the method's success. The accuracy of the angular approximations is summarized, and a series of test problems based on the C5G7 benchmarks is examined to determine the level of discretization error compared to multi-group Monte Carlo reference solutions. Errors resulting from finite element and orthogonal polynomial approximations to the spatial variables in the lateral plane as well as axial discretization are analyzed. Results for the two- and three-dimensional C5G7 benchmarks illustrate the resulting tradeoffs between accuracy and cost.

Accuracy for two-dimensional problems proves to be excellent; while in three-dimensions the axial diffusion theory limits accuracy. It is found that removing the axial diffusion limitation will require abandoning the 2D/1D formulation and basing the method on the three-dimensional even-parity transport equation, in which cross derivatives between the lateral plane and axial direction are present. Preliminary theoretical work indicates no insurmountable impediments to the development of such a fully three-dimensional pin-resolved variational nodal method.

I. INTRODUCTION

The objective of this work is to assess the approximations contained in generalizing the variational nodal method (VNM) implemented in the VARIANT code [1] for application to pin-resolved whole-core PWR problems. A 2D/1D VNM method without spatial homogenization has been formulated and implemented in the PANX (Purdue - Argonne - Northwestern - Xi'an) code [2-4]. It employs diffusion theory in the axial direction, combined with two-dimensional transport in the x-y plane. Unlike 2D/1D MOC methods, this approach does not require iteration between the x-y plane and the axial direction [5, 6]. In our initial work, we employed the standard spherical harmonics method [2]. More recently [3, 4], we have made two refinements to improve accuracy and to reduce computational cost: First, the even-parity integral method [7] within the nodes reduces the computational effort required to form the response matrices. Second, the use of quasi-reflected interface conditions [8] reduces the dimension of the resulting response matrices and therefore the CPU time required to solve the resulting equations. As a result we have successfully utilized PANX 2D/1D model to solve two- and three-dimensional C5G7 benchmark problems [9]. In what follows we report on efforts to further increase the accuracy and reduce the computational cost of 2D/1D VNM pin-resolved calculations.

In section II we update the theory to include a more streamlined implementation of the quasi-reflected interface conditions than is contained in reference [4]. Section III first examines refinement of key spatial approximations on a series of small two-dimensional test problems to determine their effects on cost and accuracy, and then applies the results to the two-dimensional C5G7 benchmark. Retaining the axial diffusion approximation, we then turn to the 2D/1D formulation. We first test it on a small problem to analyze the convergence properties of axial mesh refinement and axial interface approximations. Then the refined approximations are applied to the three-dimensional, C5G7 benchmark problem to evaluate their effects. In section IV we discuss the results and point to future research directions.

II. THEORY

The response matrices employed in this work are derived from the 2D/1D even parity approximation to the within-group transport equation, detailed elsewhere [4]:

$$-\hat{\Omega} \cdot \vec{\nabla}_p \sigma^{-1} \hat{\Omega} \cdot \vec{\nabla}_p \psi^+ - \hat{\Omega} \cdot \vec{\nabla}_z \sigma^{-1} \hat{\Omega} \cdot \vec{\nabla}_z \phi + \sigma \psi^+ = \sigma_s \phi + q \quad (1)$$

where ψ^+ and ϕ are the even-parity angular flux and scalar flux, σ and σ_s are transport corrected total and isotropic scattering cross sections, and q is the group source. The

planar and axial gradients are defined by $\vec{\nabla}_p = \hat{i} \partial / \partial x + \hat{j} \partial / \partial y$ and $\vec{\nabla}_z = \hat{k} \partial / \partial z$. Thus Eq. (1) differs from its three-dimensional equivalent in that the axial gradients operate only on the scalar flux, and the cross derivatives between the lateral plane and the axial direction have been eliminated. If ψ^+ , and thus ϕ , is independent of z , the two dimensional transport equation is obtained; besides, if they are independent of x and y , then Eq. (1) may be integrated over angle to obtain a one-dimensional diffusion equation. If diffusion holds in all three dimensions, integrating Eq. (1) over angle results in the three-dimensional diffusion equation since $\phi = \int d\Omega \psi^+$.

The variational functional corresponding to Eq. (1) is

$$F[\psi^+, \psi^-] = \sum_v F_v[\psi^+, \psi^-] \quad (2)$$

where the problem domain is the superposition of the nodal volumes V_v . The nodal functional is

$$\begin{aligned} F_v[\psi^+, \psi^-] = & \int_v dV \left[\int d\Omega \left[\sigma^{-1} (\hat{\Omega} \cdot \vec{\nabla}_p \psi^+)^2 + \right. \right. \\ & \left. \left. (3\sigma)^{-1} (\nabla_z \phi)^2 + \sigma \psi^{+2} \right] - \right. \\ & \left. \sigma_s \phi^2 - 2\phi q \right] + \\ & 2 \int_v dz \int_v d\Lambda \int d\Omega \hat{n}_p \cdot \hat{\Omega} \psi^+ \psi^- + \\ & 2 \int_v dA (\phi j_{z+}|_+ + \phi j_{z-}|_-) \end{aligned} \quad (3)$$

In local coordinates, the nodal volume is defined in $-\Delta z / 2 \leq z \leq \Delta z / 2$, the planar area is $A = \Delta x \Delta y$, \hat{n}_p being the outward normal to the lateral interfaces extending over the periphery Γ ; ψ^- is the odd-parity flux, and $j_{\pm z}$ are axial currents.

Requiring this functional to be stationary with respect to variations in ψ^+ within V_v , yields Eq. (1) as the Euler-Lagrange equation. Across the interfaces, ψ^- and $j_{\pm z}$ are defined to be continuous. Requiring Eq. (3) to be stationary with respect to variations in ψ^- and $j_{\pm z}$, yields additional continuity conditions across lateral and axial interfaces.

1. DISCRETIZATION

We discretize Eq. (3) as follows. To allow the use of the even-parity integral equation within the node we approximate the spatial distribution of the even-parity flux by

$$\psi^+(\vec{r}, \hat{\Omega}) \approx \underline{f}_z^T(z) \otimes \underline{g}^T(x, y) \underline{\psi}(\hat{\Omega}) \quad (4)$$

Correspondingly, the scalar flux is

$$\phi(\vec{r}) = \underline{f}_z^T(z) \otimes \underline{g}^T(x, y) \underline{\phi} \quad (5)$$

where $\phi = \int d\Omega \psi^+(\hat{\Omega})$. The axial distribution is approximated by $\underline{f}_z(z)$, a set of orthonormal polynomials governed by

$$\int \underline{f}_u(u) \underline{f}_u^T(u) du = \underline{I}_u \quad u = x, y, z \quad (6)$$

and $\underline{g}(x, y)$ is a vector of continuous finite element trial functions. Within a node the cross sections are independent of z and piecewise constants in x and y . We employ quadratic triangular and quadrilateral iso-parametric finite elements so that the element boundaries faithfully map curved material interfaces. Fig. 1 illustrates three finite element meshes used to represent a fuel pin cells in the C5G7 calculations in the following section.

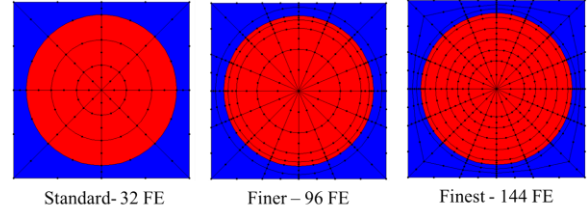


Fig. 1. Three Quadratic Finite Element Grids for a Fuel Pin Cell

On the axial interfaces the current is approximated by

$$j_{z\pm}(x, y) \approx \underline{h}^T(x, y) \chi_{z\pm} \quad (7)$$

where $\underline{h}(x, y)$ is a vector of piecewise constants within the area A_i covered by the i^{th} finite element $h_i(x, y) = A_i^{-1/2}$, and is set equal to zero elsewhere. On the lateral surfaces

$$\begin{aligned} \psi^-(\zeta, \hat{\Omega}) \approx & \underline{y}_\gamma^T(\hat{\Omega}) \otimes \underline{f}_\gamma^T(\zeta) \underline{\chi}_\gamma + \\ & \underline{y}_{\gamma o}^T(\hat{\Omega}) \otimes \underline{f}_\gamma^T(\zeta) \underline{\chi}_{\gamma o} \quad \zeta = y, x \end{aligned} \quad (8)$$

where $\gamma = 1, 2, 3, 4$ correspond to the left, right, bottom and top interfaces, correspondingly $\gamma = -x, +x, -y, +y$. The vector $\underline{f}_\gamma(\zeta)$ consists of orthonormal functions defined by Eq. (6). The spherical harmonics vectors $\underline{y}_\gamma(\hat{\Omega})$ and $\underline{y}_{\gamma o}(\hat{\Omega})$ contain only the cosine series of odd-parity spherical harmonics: $\underline{y}_\gamma(\hat{\Omega})$ is a low-order P_n vector, say with $n=1$ or 3. $\underline{y}_{\gamma o}(\hat{\Omega})$ is a high-order vector ranging from $n+2$ up to some larger value of n .

However, we apply reflected interface conditions to the high-order expansions by deleting the Y_m terms with even m from the vector [10]; we employ the subscript o to indicate that only the odd m terms are included in the expansion. Since Eq. (1) maintains two-dimensional symmetry in angle, the spherical harmonics vectors include only the cosine series rotated to align the polar axis with the outward normal \hat{n}_γ and an azimuthal angle measured from the lateral plane.

Inserting the trial functions of Eq. (4), (5), (7) and (8) into Eq. (3) yields the discretized functional

$$F[\underline{\psi}, \underline{\chi}_\gamma, \underline{\chi}_z] = \int d\Omega \underline{\psi}^T(\hat{\Omega}) \underline{A}(\hat{\Omega}) \underline{\psi}(\hat{\Omega}) - \underline{\phi}^T \left[\underline{I}_{=z} \otimes \underline{F}_{=s} - \underline{P}_{=zz} \otimes \underline{F}_{=-} \right] \underline{\phi} - 2\underline{\phi}^T \underline{I}_{=z} \otimes \underline{F}q + 2 \sum_\gamma \int d\Omega \underline{\psi}^T(\hat{\Omega}) \underline{E}_\gamma(\hat{\Omega}) \underline{\chi}_\gamma + 2 \sum_\gamma \int d\Omega \underline{\psi}^T(\hat{\Omega}) \underline{E}_{\gamma o}(\hat{\Omega}) \underline{\chi}_{\gamma o} + 2 \sum_{z'} \underline{\phi}^T \underline{E}_{=z'} \underline{j}_{z'} \quad (9)$$

where

$$\underline{A}(\hat{\Omega}) = \underline{I}_{=z} \otimes \sum_{x,y} \Omega_x \Omega_y P_{xy} + \underline{I}_{=z} \otimes \underline{F}_{=t} \quad (10)$$

$$\underline{E}_\gamma(\hat{\Omega}) = \Omega_\gamma \underline{i}_o \underline{y}_\gamma^T(\hat{\Omega}) \otimes \underline{D}_\gamma \quad (11)$$

$$\underline{E}_{\gamma o}(\hat{\Omega}) = \Omega_\gamma \underline{i}_o \underline{y}_{\gamma o}^T(\hat{\Omega}) \otimes \underline{D}_\gamma \quad (12)$$

$$\underline{E}_{=z} = \underline{f}_{=z} \Big|_{\pm} \otimes \underline{D}_{=z} \quad (13)$$

$$\underline{i}_o^T = [1 \ 0 \ \dots \ 0] \quad (14)$$

and the matrices containing integrals over the spatial trial functions are defined in Table 1. The spatial integrals are evaluated numerically using standard finite element techniques. Based on preliminary investigations [4], the group source q is taken to be piecewise constant, with a unique value for each of the finite element areas in the x - y plane, but to vary axially with $f_z(z)$.

Table 1 Spatial Integrals
$\underline{P}_{xy} = \int dx dy \sigma^{-1} (\nabla_x \underline{g}) (\nabla_y \underline{g}^T)$
$\underline{P}_{zz} = \int dz (\nabla_z \underline{f}_{=z}) (\nabla_z \underline{f}_{=z}^T)$
$\underline{D}_\gamma = \sqrt{\Delta z} \int d\Gamma \underline{g} \Big _\gamma \underline{f}_\gamma^T \quad \gamma = x, y$
$\underline{D}_{=z} = \int dx dy \underline{g} \underline{h}^T$
$\underline{F}_{=} = \int dx dy \underline{g} \underline{g}^T$
$\underline{F}_{=-} = \int dx dy (3\sigma)^{-1} \underline{g} \underline{g}^T$
$\underline{F}_{=x} = \int dx dy \sigma_x \underline{g} \underline{g}^T \quad x = a, t, s$

We next re-group the terms in Eq. (11) and Eq. (12) by low- and high-order terms:

$$\underline{\chi}_l^T = \left[\underline{\chi}_{\gamma=1}^T \quad \underline{\chi}_{\gamma=2}^T \quad \underline{\chi}_{\gamma=3}^T \quad \underline{\chi}_{\gamma=4}^T \quad \underline{j}_{z+}^T \quad \underline{j}_{z-}^T \right] \quad (15)$$

$$\underline{E}_l(\hat{\Omega}) = \begin{bmatrix} \underline{E}_{\gamma=1}(\hat{\Omega}) \\ \underline{E}_{\gamma=2}(\hat{\Omega}) \\ \underline{E}_{\gamma=3}(\hat{\Omega}) \\ \underline{E}_{\gamma=4}(\hat{\Omega}) \\ \underline{E}_{=+z} \\ \underline{E}_{=-z} \end{bmatrix}^T \quad (16)$$

$$\underline{\chi}_o^T = \left[\underline{\chi}_{\gamma o=1}^T \quad \underline{\chi}_{\gamma o=2}^T \quad \underline{\chi}_{\gamma o=3}^T \quad \underline{\chi}_{\gamma o=4}^T \right] \quad (17)$$

$$\underline{E}_o(\hat{\Omega}) = \begin{bmatrix} \underline{E}_{\gamma o=1}(\hat{\Omega}) \\ \underline{E}_{\gamma o=2}(\hat{\Omega}) \\ \underline{E}_{\gamma o=3}(\hat{\Omega}) \\ \underline{E}_{\gamma o=4}(\hat{\Omega}) \end{bmatrix}^T \quad (18)$$

Thus the discretized functional becomes

$$F[\underline{\psi}, \underline{\chi}_l, \underline{\chi}_o] = \int d\Omega \underline{\psi}^T(\hat{\Omega}) \underline{A}(\hat{\Omega}) \underline{\psi}(\hat{\Omega}) - \underline{\phi}^T \left[\underline{I}_{=z} \otimes \underline{F}_{=s} - \underline{P}_{=zz} \otimes \underline{F}_{=-} \right] \underline{\phi} - 2\underline{\phi}^T \underline{I}_{=z} \otimes \underline{F}q \quad (19) + 2 \int d\Omega \underline{\psi}^T(\hat{\Omega}) \underline{E}_l(\hat{\Omega}) \underline{\chi}_l + 2 \int d\Omega \underline{\psi}^T(\hat{\Omega}) \underline{E}_o(\hat{\Omega}) \underline{\chi}_o$$

2. VARIATIONAL PROCEDURES

We require the discretized functional, Eq. (19), to be stationary with respect to variation in $\underline{\psi}(\hat{\Omega})$ yielding

$$\underline{A}(\hat{\Omega}) \underline{\psi}(\hat{\Omega}) - \left[\underline{I}_{=z} \otimes \underline{F}_{=s} - \underline{P}_{=zz} \otimes \underline{F}_{=-} \right] \underline{\phi} = \underline{I}_{=z} \otimes \underline{F}q - \underline{E}_l(\hat{\Omega}) \underline{\chi}_l - \underline{E}_o(\hat{\Omega}) \underline{\chi}_o \quad (20)$$

which we solve for the even parity flux vector:

$$\underline{\psi}(\hat{\Omega}) = \underline{A}(\hat{\Omega})^{-1} \left\{ \left[\underline{I}_{=z} \otimes \underline{F}_{=s} - \underline{P}_{=zz} \otimes \underline{F}_{=-} \right] \underline{\phi} + \underline{I}_{=z} \otimes \underline{F}q \right\} - \underline{A}(\hat{\Omega})^{-1} \left\{ \underline{E}_l(\hat{\Omega}) \underline{\chi}_l + \underline{E}_o(\hat{\Omega}) \underline{\chi}_o \right\} \quad (21)$$

To proceed, we first eliminate the scalar flux from the right side of this equation by first integrating Eq. (21) over angle to obtain

$$\underline{\phi} = \underline{H} \tilde{\underline{F}} \underline{\phi} + \underline{H} \tilde{\underline{F}} q - \underline{M}_l \underline{\chi}_l - \underline{M}_o \underline{\chi}_o \quad (22)$$

where the matrices are defined in Table 2. The integrals over angle are evaluated using high-order square Chebyshev-Legendre cubature.

Table 2 Angular Integrals
$\underline{H} = \int d\Omega \underline{A}(\hat{\Omega})^{-1}$
$\underline{M}_l = \int d\Omega \underline{A}(\hat{\Omega})^{-1} \underline{E}_l(\hat{\Omega})$
$\underline{M}_o = \int d\Omega \underline{A}(\hat{\Omega})^{-1} \underline{E}_o(\hat{\Omega})$
$\underline{L}_{ll} = \int d\Omega \underline{E}_l(\hat{\Omega})^T \underline{A}(\hat{\Omega})^{-1} \underline{E}_l(\hat{\Omega})$
$\underline{L}_{lo} = \int d\Omega \underline{E}_l(\hat{\Omega})^T \underline{A}(\hat{\Omega})^{-1} \underline{E}_o(\hat{\Omega})$
$\underline{L}_{ol} = \int d\Omega \underline{E}_o(\hat{\Omega})^T \underline{A}(\hat{\Omega})^{-1} \underline{E}_l(\hat{\Omega})$
$\underline{L}_{oo} = \int d\Omega \underline{E}_o(\hat{\Omega})^T \underline{A}(\hat{\Omega})^{-1} \underline{E}_o(\hat{\Omega})$
$\tilde{\underline{F}}_{=s} = \underline{I}_{=z} \otimes \underline{F}_{=s} - \underline{P}_{=zz} \otimes \underline{F}_{=-}$
$\tilde{\underline{F}} = \underline{I}_{=z} \otimes \underline{F}_{=}$

We next define

$$\underline{\underline{Z}} = \underline{\underline{I}} - \underline{\underline{H}}\underline{\underline{F}} \quad (23)$$

and solve Eq. (22) for the scalar flux

$$\underline{\underline{\phi}} = \underline{\underline{Z}}^{-1} \underline{\underline{H}}\underline{\underline{F}}\underline{\underline{q}} - \underline{\underline{Z}}^{-1} \left\{ \underline{\underline{M}}_l \underline{\underline{\chi}}_l + \underline{\underline{M}}_o \underline{\underline{\chi}}_o \right\} \quad (24)$$

Inserting this expression into Eq. (21), we obtain the even-parity flux within the node in term of the group source, the odd-parity flux on the lateral interfaces, and the currents of the axial interfaces:

$$\begin{aligned} \underline{\underline{\psi}}(\hat{\Omega}) = & \underline{\underline{A}}(\hat{\Omega})^{-1} \left[\underline{\underline{I}} + \underline{\underline{F}} \underline{\underline{Z}}^{-1} \underline{\underline{H}} \right] \underline{\underline{F}}\underline{\underline{q}} - \\ & \underline{\underline{A}}(\hat{\Omega})^{-1} \left\{ \left[\underline{\underline{E}}_l(\hat{\Omega}) + \underline{\underline{F}}_s \underline{\underline{Z}}^{-1} \underline{\underline{M}}_l \right] \underline{\underline{\chi}}_l + \right. \\ & \left. \left[\underline{\underline{E}}_o(\hat{\Omega}) + \underline{\underline{F}}_s \underline{\underline{Z}}^{-1} \underline{\underline{M}}_o \right] \underline{\underline{\chi}}_o \right\} \end{aligned} \quad (25)$$

Requiring Eq. (19) to be stationary with respect to variations $\underline{\underline{\chi}}_l$ and $\underline{\underline{\chi}}_o$ yields the conditions that the following quantities must be continuous across the lateral and axial interfaces:

$$\underline{\underline{\varphi}}_l = \int d\Omega \underline{\underline{E}}_l^T(\hat{\Omega}) \underline{\underline{\psi}}(\hat{\Omega}) \quad (26)$$

and

$$\underline{\underline{\varphi}}_o = \int d\Omega \underline{\underline{E}}_o^T(\hat{\Omega}) \underline{\underline{\psi}}(\hat{\Omega}) \quad (27)$$

However, to employ the quasi-static interface conditions, we must impose the condition that for even l the Y_{lm} coefficients must vanish for odd values of m [10]. Thus

$$\underline{\underline{\varphi}}_o = 0 \quad (28)$$

Inserting Eq. (25) into Eq. (26) and (27) yields

$$\underline{\underline{\varphi}}_l = \underline{\underline{U}}_l \underline{\underline{q}} - \underline{\underline{G}}_{ll} \underline{\underline{\chi}}_l - \underline{\underline{G}}_{lo} \underline{\underline{\chi}}_o \quad (29)$$

and

$$\underline{\underline{\varphi}}_o = \underline{\underline{U}}_o \underline{\underline{q}} - \underline{\underline{G}}_{ol} \underline{\underline{\chi}}_l - \underline{\underline{G}}_{oo} \underline{\underline{\chi}}_o \quad (30)$$

Likewise, Eq. (24) may be written more compactly as

$$\underline{\underline{\phi}} = \underline{\underline{V}}_l \underline{\underline{q}} - \underline{\underline{C}}_l \underline{\underline{\chi}}_l - \underline{\underline{C}}_o \underline{\underline{\chi}}_o \quad (31)$$

where the matrices are defined in Table 3.

We next solve $\underline{\underline{\chi}}_o$ in Eq. (30) and eliminate it from Eq. (29) and (31). Hence we have

$$\underline{\underline{\varphi}} = \underline{\underline{U}}\underline{\underline{q}} - \underline{\underline{G}}\underline{\underline{\chi}} \quad (32)$$

and

$$\underline{\underline{\phi}} = \underline{\underline{V}}\underline{\underline{q}} - \underline{\underline{C}}\underline{\underline{\chi}} \quad (33)$$

where the resulting matrices are given in Table 3.

Table 3 Matrix Relationships	
$\underline{\underline{V}} = \underline{\underline{Z}}^{-1} \underline{\underline{H}} \underline{\underline{F}}$	$\underline{\underline{C}}_i = \underline{\underline{Z}}^{-1} \underline{\underline{M}}_i \quad i, j = l, o$
$\underline{\underline{U}}_i = \underline{\underline{M}}_i^T \left[\underline{\underline{I}} + \underline{\underline{F}}_s \underline{\underline{Z}}^{-1} \underline{\underline{H}} \right] \underline{\underline{F}}$	$\underline{\underline{G}}_{ij} = \underline{\underline{L}}_{ij} + \underline{\underline{M}}_i^T \underline{\underline{F}}_s \underline{\underline{Z}}^{-1} \underline{\underline{M}}_j$
$\underline{\underline{U}} = \underline{\underline{U}}_l - \underline{\underline{G}}_{lo} \underline{\underline{G}}_{oo}^{-1} \underline{\underline{U}}_o$	$\underline{\underline{G}} = \underline{\underline{G}}_{ll} - \underline{\underline{G}}_{lo} \underline{\underline{G}}_{oo}^{-1} \underline{\underline{G}}_{ol}$
$\underline{\underline{V}} = \underline{\underline{V}}_l - \underline{\underline{C}}_{=o} \underline{\underline{G}}_{=oo}^{-1} \underline{\underline{U}}_o$	$\underline{\underline{C}} = \underline{\underline{C}}_l - \underline{\underline{C}}_{=o} \underline{\underline{G}}_{=oo}^{-1} \underline{\underline{G}}_{=ol}$

3. RESPONSE MATRIX EQUATIONS

To recast Eq. (32) in response matrix form we utilize a transformation to variables, which in diffusion theory reduces to the partial currents:

$$\underline{\underline{j}}^\pm = \frac{1}{4} \underline{\underline{\varphi}}^\pm \pm \frac{1}{2} \underline{\underline{\chi}} \quad (34)$$

where $\underline{\underline{j}}^-$ and $\underline{\underline{j}}^+$ correspond respectively to incoming and outgoing neutron currents. Changing variables to write Eq. (32) in terms of $\underline{\underline{j}}^\pm$ yields the response matrix equation,

$$\underline{\underline{j}}^+ = \underline{\underline{B}}\underline{\underline{q}} + \underline{\underline{R}} \underline{\underline{j}}^- \quad (35)$$

where

$$\underline{\underline{B}} = \frac{1}{2} \left[\frac{1}{2} \underline{\underline{G}} + \underline{\underline{I}} \right]^{-1} \underline{\underline{U}} \quad (36)$$

and

$$\underline{\underline{R}} = \underline{\underline{I}} - 2 \left[\frac{1}{2} \underline{\underline{G}} + \underline{\underline{I}} \right]^{-1} \quad (37)$$

With the partial currents known, the scalar flux may be determined in terms of the partial currents from Eq. (33):

$$\underline{\underline{\phi}} = \underline{\underline{V}}\underline{\underline{q}} - \underline{\underline{C}} \left(\underline{\underline{j}}^+ - \underline{\underline{j}}^- \right) \quad (38)$$

III. RESULTS

In this section, seven group cross sections from the C5G7 benchmark are employed in all the calculations, and corresponding multi-group Monte Carlo solutions are taken as references. To begin, the PANX code is applied to review our previous work, where angular approximations were examined using a fixed set of spatial approximation. Second, we examine the refinement of spatial approximations. In this process, two-dimensional single cell problems are used to assess the adequacy of the finite element mesh and the interface polynomials. Then the mesh and polynomial order thus obtained are applied in the unrodded two-dimensional C5G7 problem. Furthermore, in three dimensions, we employ a four pin problem to examine convergence of the axial grid in conjunction with the coupling of the finite element meshes at the axial interfaces. We then employ the aforementioned finding to the unrodded and rodded three-dimensional C5G7 benchmarks.

1. ANGULAR APPROXIMATIONS

In our studies of angular approximations, the spatial approximations are fixed: we use 32 quadratic finite elements (32QFE) as shown in Fig. 1 within the node and 2nd order orthogonal polynomials on the lateral interfaces. Three different forms of the PANX code are employed. In its initial form, standard spherical harmonics expansions were used within the node as well as on the node interfaces. This form has been abandoned lately since memory and CPU requirements became prohibitive to achieve

sufficiently high order spherical harmonic approximations. PANX_I is the integral method detailed in Section II, without the use of quasi-reflected boundary conditions, and PANX_IQ_n is the integral method with P_n conditions on the interface with quasi-reflected interface conditions extending to some higher order P_m . For brevity we will often refer to these simply as P_m - P_n approximations. All angular integrals are evaluated using 25×25 square Legendre-Chebyshev cubature.

Results for the two-dimensional unrodded C5G7 problem are shown in Fig. 2 for the three forms of the PANX code, where the high-order P_m interface conditions are plotted from P_1 through P_{23} . It was concluded that the P_{23} - P_3 approximation provided sufficient accuracy

compared to the reference multi-group Monte Carlo solution to justify its use in subsequent calculations.

Fig 3 is an analogous plot for the three-dimensional unrodded C5G7 benchmark. We employ the same $32\text{QFE}/2^{\text{nd}}$ order spatial approximations in the x-y planes. A quadratic polynomial approximates the axial dependence of the even-parity flux within the nodes, and the axial domain is divided into 18 segments. For the three dimensional problem, the solutions converges to a value significantly lower than the multi-group Monte Carlo reference solution. We attribute this primarily to the use of axial diffusion theory in the 2D/1D formulation. We again conclude that the P_{23} - P_3 approximation is adequate for subsequent calculations.

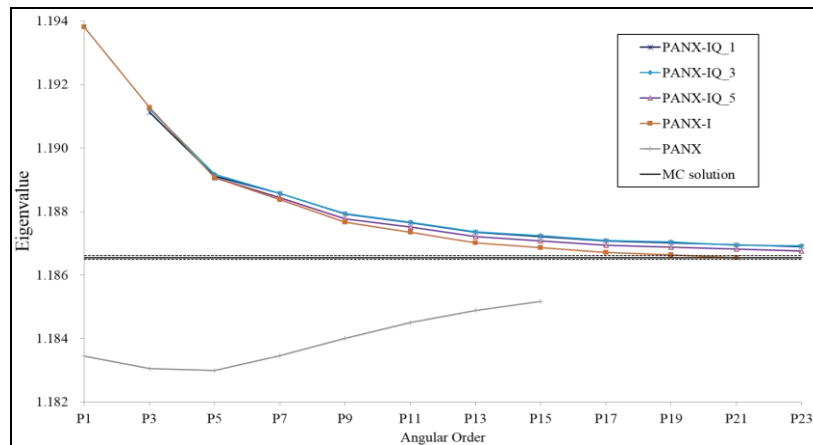


Fig. 2. Eigenvalue vs. P_m Approximation for the Unrodded 2D C5G7 Benchmark

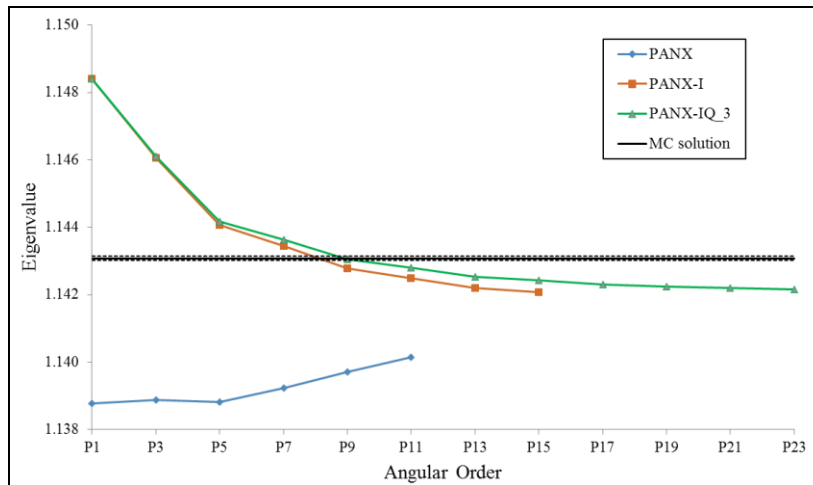


Fig. 3. Eigenvalue vs. P_m Order for the 3D Unrodded C5G7 Benchmark

2. SPATIAL APPROXIMATIONS – TWO DIMENSIONS

To examine the finite element trial functions, $\underline{g}(x, y)$ in Eq. (4), and the lateral interface polynomials, $\underline{f}_y(\zeta)$ in Eq. (8) are considered using the MOX (8.7% enrichment)

and UO_2 pin cells. The 32 QFE, 96 QFE and 144 QFE grids depicted in Fig. 1 with 2^{nd} , 4^{th} and 6^{th} order orthogonal polynomials on the interfaces are compared, while in earlier publications only $32\text{QFE}/2^{\text{nd}}$ order was used. The Monte Carlo reference values are $k = 1.32557$ and 1.17472 with 99% confidence limits of 7 pcm and 3 pcm. The infinite lattice pcm errors in the eigenvalues are shown in Fig. 4 for

the nine combinations of mesh. Cancellation of error is clearly present in the 2nd order polynomial results, for the eigenvalue error becomes worse as the finite element mesh is refined. For the 4th and 6th order polynomials, the errors are small and decrease with the refinement of the finite element mesh. Based on these results, we conclude that the 96QFE/4th mesh provides sufficient accuracy.

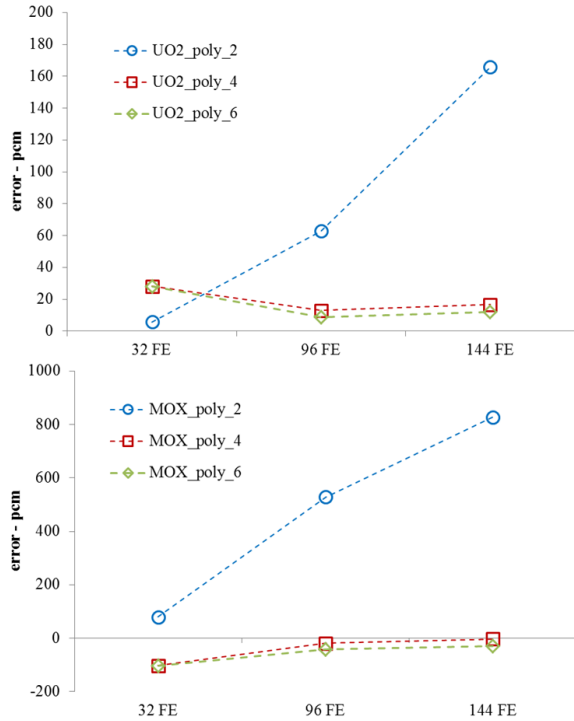


Fig. 4. UO₂ and MOX Pin Cell Eigenvalue Errors

To study the effects of mesh refinement in a non-uniform problem, we employ the four pin configuration shown in Fig. 5. It consists of two MOX (8.7% enrichment) and two UO₂ pin cell with reflected conditions on the outer boundaries. Results are shown in Table 4 for the eigenvalue and the power ratio between pins for the 32QFE/quadratic and the 96QFE/quartic approximations. P_{23-P_1} , P_{23-P_3} , and P_{23-P_5} angular interface conditions are implemented to show the effects of employing different quasi-reflected interface conditions.

In this case, the Monte Carlo reference values are $k = 1.22919 \pm 2$ pcm and the power ratio being $1.8044 \pm 0.03\%$. It is observed that the coarser spatial approximation results in 50-60 pcm positive error, while the P_{23-P_1} approximation causes a comparable negative error. Besides, the differences between P_{23-P_3} and P_{23-P_5} approximation using both spatial approximations are only a few pcm, indicating the adequacy of the P_{23-P_3} interface approximation. In addition, there is little difference in the power ratio between different spatial approximations, while refining the angular interface approximation from P_{23-P_1} to P_{23-P_3} reduces the error by nearly an order of magnitude,

whereas refining it to P_{23-P_5} produces insignificant improvements.

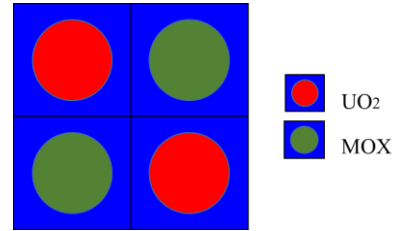


Fig. 5. The Four Pin Configuration with Reflected Boundary Conditions

		P_{23-P_1}	P_{23-P_3}	P_{23-P_5}
Eigenvalue	32QFE /quadratic	1.22920	1.22975	1.22972
	96QFE /quartic	1.22854	1.22924	1.22919
Error - pcm	32QFE /quadratic	1	56	53
	96QFE /quartic	-65	5	0
Power Ratio (MOX/UO2)	32QFE /quadratic	1.8404	1.8108	1.8082
	96QFE /quartic	1.8426	1.8102	1.8075
Error - %	32QFE /quadratic	2.00	0.35	0.21
	96QFE /quartic	2.12	0.32	0.17

Table 5 shows results for the unrodded 2D C5G7 problem comparing the 96QFE/4th P_{23-P_3} to the 32QFE/2nd P_{23-P_3} used in earlier calculations. To assess the overall pin power distribution, the pin power error of the maximum power pin-cell (Max Pin), the average pin power error (AVG), the root-mean-square (RMS) of the pin power distribution, and the mean relative pin power error (MRE) are included. Distinct improvement is shown in the pin power results while the eigenvalue remains essentially unchanged. As expected, the refined spatial approximations add considerably to the computation times.

		32QFE /quadratic	96QFE /quartic
Eigenvalue error /pcm		18	20
Pin power error /%	MAX	-0.30	-0.08
	AVG	0.24	0.14
	RMS	0.27	0.18
	MRE	0.22	0.12
CPU time /h	Total	0.12	1.75
	Formation*	0.10	1.70
	Solution	0.02	0.04
Memory /GB		0.07	0.12

* Response matrix formation

3. SPATIAL APPROXIMATIONS – THREE DIMENSIONS

To examine the effects of refining axial meshes and of changing axial interface approximation we employed the two-dimensional 4 pin configuration illustrated in Fig. 5. The extension has an axial length of 42.84 cm, which equals the length of the active region in the C5G7 benchmark, with a vacuum boundary condition at one end and a reflected condition on the other. To reduce computing efforts, in these calculations we employ 32QFE mesh with 2nd order polynomials on the x and y interfaces. The angular approximation is P_{23} - P_3 . In three-dimensional calculations to date [4], the piecewise constant function, $h(x, y)$ in Eq. (7), has been employed with one piecewise constant per finite element. For clarity, each of these constant is referred to an axial interface zone. As indicated in Fig. 6, we considered 1, 2, and 4 zones as well as the standard 32 zone axial interface condition. In all four cases, we retain 32 quadratic finite elements to approximate the lateral plane distribution of the even-parity flux within the node.

Plots are shown in Fig. 7 for each of the four zone structures where the length of the fuel pins are divided into increasing numbers of increments, thus decreasing the axial dimension of the nodes. The graph displays two striking results. First, the one-zone results do not converge as the axial mesh is refined while the others do converge. We attribute the non-convergence to the artificial smearing of fuel and coolant at each of the axial interfaces, which occur at shorter intervals as the axial mesh is refined. Second, as long as there is no fuel-coolant smearing, i.e. as long as there are two or more zones, the number of zones has a nearly imperceptible influence on the eigenvalue. Based on these results, we have replaced the 32 zone model used to date with the two-zone model in applying PANX to the three-dimensional C5G7 benchmarks; it results in significant reduction in computational effort while causing negligible loss of accuracy.

Table 6 displays the results for the three-dimensional C5G7 benchmarks employing 2 axial interface zones and 18 axial segments. To show the effects of spatial mesh refinement, both 32QFE/2nd order and 96QFE/4th order approximations are employed. All calculations were performed on a Xeon X7560 CPU. Sixteen thread OpenMP was applied to the response matrix formation with efficiencies between 70 and 80 percent.

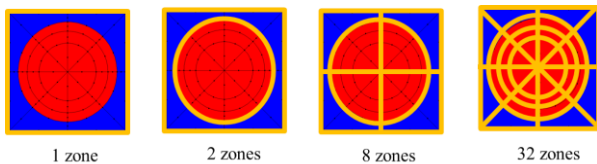


Fig. 6. Axial Interface Piecewise Constant Zones

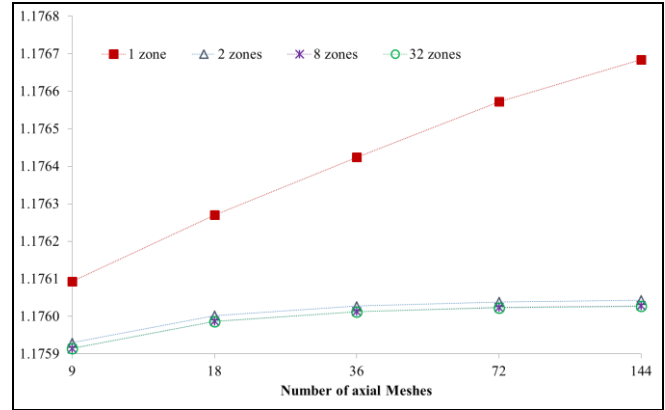


Fig. 7. Eigenvalue Convergence vs. Number of Planes for 4 Pin-cell Problem

DISCUSSION

The preceding sections present the continued development of a variational nodal method based on a 2D/1D approximation of the even-parity neutron transport equation for pin-resolved analysis of pressurized water reactors. In earlier work emphasis was placed on determining the refinement of the angular approximations needed to achieve accurate solutions. Much less effort went into determining the sensitivity of the results to refinement of spatial discretization. In this paper we utilize the C5G7 benchmark problems to examine the cost-accuracy tradeoffs in refining the finite element mesh within the node, the orthogonal polynomial representation of the lateral interface variables, and the axial mesh and interface approximations.

After examining spatial and angular truncation errors, we conclude that the largest errors remain in three-dimensional problems, and that these stem from the axial diffusion approximation in the 2D/1D approximation to the even-parity transport equation. We made a concerted effort to remove the axial diffusion limitation: $\bar{\nabla}_z \phi(\vec{r})$ is replaced by $\bar{\nabla}_z \psi(\vec{r}, \hat{\Omega})$ in Eq. (1) and subsequent equations in order to incorporate P_n or SP_n approximations in the axial direction. Doing so caused no perceptible change in the results. We thus conclude that our 2D/1D simplification must be abandoned, and the three-dimensional even-parity transport equation, which includes cross derivatives between the lateral plane and the axial direction, should be employed. We have formulated such a three-dimensional variational nodal method and are proceeding to implement it in the PANX code. Work is also beginning on code parallelizing to reduce costs and enable the treatment of full reactor cores.

ACKNOWLEDGEMENTS

This work is supported by the China Scholarship Council, the National Natural Science Foundation of China (No. 11305123), and the U.S. Department of Energy, Office

of Science, Basic Energy Sciences, under contract number DE-AC02-06CH11357. The U.S. Government retains for itself, and others acting on its behalf, a paid-up nonexclusive, irrevocable worldwide license in said article to reproduce, prepare derivative works, distribute copies to the public, and perform publicly and display publicly, by or on behalf of the Government.

REFERENCES

1. M. A. SMITH, E. E. LEWIS and E. R. SHEMON, "DIF3D-VARIANT 11.0: A Decade of Updates, ANL/NE-14/1, Argonne National Laboratory (January, 2014).
2. TENGFEI ZHANG, E. E. LEWIS, M. A. SMITH and W. S. YANG, "A Variational Nodal Approach to 2D/1D Pin Resolved Neutron Transport: II Spherical Harmonics," *Trans. Am. Nucl. Soc.* **114**, 773 (2016).
3. TENGFEI ZHANG, E. E. LEWIS, M. A. SMITH, W. S. YANG, and H. WU, "Variational Nodal 2D/1D Transport/Diffusion Solutions of the C5G7 Benchmark Problems," *Trans. Am. Nucl. Soc.* **115**, 1118 (2016).
4. TENGFEI ZHANG, E. E. LEWIS, M. A. SMITH, W. S. YANG, and H. WU, "A Variational Nodal Approach to 2D/1D Pin Resolved Neutron Transport for Pressurized Water Reactors," *Nucl. Sci. Eng.* **186** (2017). (accepted for publication).
5. H. G. JOO, J. Y. CHO, K. S. KIM, C. C. LEE and S. Q. ZEE., "Methods and performance of a three-dimensional whole-core transport code DeCART," Proc. PHYSOR 2004, Chicago, IL, April 25-29, 2004, American Nuclear Society (2004).
6. B KOCHUNAS, B. COLLINS, T. J. DOWNAR and W. R. MARTIN, "Overview of Development and Design of MPACT: Michigan Parallel Characteristics Transport Code," Proc. M&C 2013, Sun Valley, ID, USA, May 5-9.
7. M. A. SMITH, E. E. LEWIS, G. PALMIOTTI and N. TSOULFANIDIS, "An Integral Form of the Variational Nodal Method" *Nucl. Sci. Eng.* **146**, 141 (2004).
8. E. E. LEWIS, M. A. SMITH and G. PALMIOTTI, "A New Paradigm for Local-Global Coupling in Whole-Core Neutron Transport," *Nucl. Sci. Eng.* **161**, 279 (2009).
9. M. A. SMITH, E. E. LEWIS, and B. C. NA, "Benchmark on Deterministic Transport Calculations without Spatial Homogenization: A 2-D/3-D MOX Fuel Assembly 3-D Benchmark," NEA/NSC/DOC (2003)16.
10. E. E. LEWIS, C.B. CARRICO and G. PALMIOTTI, "Variational Nodal Formulation for the Spherical Harmonics Equations," *Nucl. Sci. Eng.*, **122**, 194 (1996).

		Un-rodged		Rodded A		Rodded B	
		32QFE /quadratic	96QFE /quartic	32QFE /quadratic	96QFE /quartic	32QFE /quadratic	96QFE /quartic
Eigenvalue error /pcm		-107	-80	-157	-173	-227	-238
Axially integrated pin power error /%	MAX	-0.62	0.25	-0.98	0.70	-0.82	-0.53
	AVG	0.44	0.23	0.55	0.40	0.57	0.41
	RMS	0.51	0.29	0.62	0.46	0.66	0.49
	MRE	0.40	0.21	0.53	0.37	0.57	0.40
Slice 1 pin power error /%	MAX	-1.18	1.04	-1.62	1.37	-2.59	-2.21
	AVG	0.48	0.60	0.57	0.48	0.8	0.70
	RMS	0.62	0.69	0.73	0.62	1.09	0.95
	MRE	0.29	0.34	0.37	0.32	0.61	0.54
Slice 2 pin power error /%	MAX	-0.84	0.61	-1.03	0.69	-0.12	0.25
	AVG	0.44	0.31	0.56	0.41	0.44	0.42
	RMS	0.55	0.38	0.65	0.50	0.53	0.53
	MRE	0.17	0.13	0.21	0.15	0.13	0.14
Slice 3 pin power error /%	MAX	1.05	2.20	2.81	3.06	3.71	3.87
	AVG	1.68	2.15	1.86	1.73	2.81	2.63
	RMS	1.72	2.19	1.96	1.90	2.88	2.73
	MRE	0.32	0.43	0.30	0.29	0.36	0.34
CPU time /h	Total	0.69	8.64	0.62	7.81	0.61	8.43
	Formation*	0.14	7.72	0.12	6.71	0.13	7.11
	Solution	0.55	0.92	0.50	1.10	0.48	1.32
Memory /GB		3.12	7.70	2.94	7.85	3.12	7.88

* Response matrix formation